Shadow Nanosphere Lithography: Simulation and Experiment

ARTICLE *in* NANO LETTERS · JULY 2004

Impact Factor: 13.59 · DOI: 10.1021/nl049361t

NANO LETTERS

2004
Vol. 4, No. 7
1359−1363

Shadow Nanosphere Lithography: Simulation and Experiment

A. Kosiorek,[†] W. Kandulski,[†] P. Chudzinski,[‡] K. Kempa,[§] and M. Giersig*,[†]

Center of Advanced European Studies and Research (CAESAR), Bonn, Germany, Poznan University of Technology, Poznan, Poland, Boston College, Chestnut Hill, Massachusetts 02467

Received April 30, 2004; Revised Manuscript Received May 17, 2004

ABSTRACT

In this letter we describe the preparation of large-area, two-dimensional metallic structures using shadow nanosphere lithography. By varying the position of the substrate with respect to the evaporation source during the sample preparation, we make morphologies such as cups, rods, and wires, that are not accessible by the standard nanosphere lithography. This technique also allows for an encapsulation of the metallic structures, to prevent them from oxidation. Morphologies predicted by our computer simulations have been subsequently confirmed experimentally.

Self-assembly of the hexagonal closed-packed (hcp) monolayer of latex spheres, is a basis of the nanosphere lithography (NSL).[1−8] This technique is used for creation of masks for deposition of various materials, typically by evaporation or sputtering. It is known that NSL can be used to make honeycomb lattices of triangularly shaped islands on various substrates. Using spheres with different diameters, one can change the spacing and size of the periodically arranged islands. By annealing the samples at the temperature of about 70% of the melting point of the bulk material and adjusting the time of the thermal treatment, spherical particles can be obtained.[9] Van Duyne et al. shown that nanooverlaps, nanogaps, and nanochains can be obtained by multiple silver depositions at different deposition angles. They called this technique angle-resolved NSL.[10]

We show here that the deposited structures can become much more complex when the angle between the evaporation beam and the sample is changing during the deposition process and when the sample is simultaneously rotated during the process. We have developed computer simulations that predict the resulting structures. A variety of complex morphologies, ranging from cup-like structures to rods and wires, are possible using this technique.

The standard electron beam evaporation (EBE) system was modified to ensure control over the evaporation angle θ and the sample rotation at the same time (see Figure 1).

Theory. To predict the desired morphologies we have performed computer simulations of the process parameters.

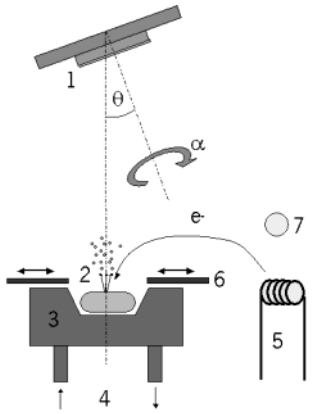

Figure 1. Schematic of the modified evaporation system. (1) sample holder, (2) evaporation source, (3) crucible, (4) water cooling system, (5) electron beam source, (6) shutter, (7) magnetic field. θ is the evaporation angle, and α the rotation angle of the sample.

These simulations require information about the mask geometry, i.e., the sphere radius R and positions of the centers of the spheres (x_i, y_i). Simulations produce the thickness $d(x,y)$ of the deposited film at each location (x,y) on the substrate. In the simulations we assume that the evaporated atoms move without scattering, away from the point source, following straight trajectories, and make the problem completely analogous to that of the geometrical optics of a moving point light source. Therefore, $d(x,y)$ can be obtained as a time average of the light intensity masked out by the PS spheres, thus the name shadow lithography. This is a good approximation as is shown by comparison with the experimental results. We fully exploit the symmetry of the hcp array of the PS spheres. A simple geometric analysis yields

* Corresponding author. E-mail: giersig@caesar.de.
[†] CAESAR.
[‡] Poznan University of Technology.
[§] Boston College.

10.1021/nl049361t CCC: $27.50
Published on Web 06/05/2004

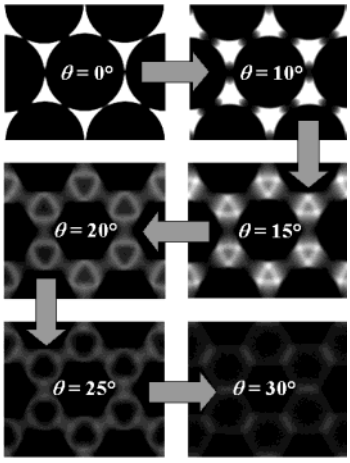

Figure 2. Simulation results for the evaporation through an hcp mask of ordered spheres, with evaporation angles θ varying from 0° (perpendicular evaporation) to 30°.

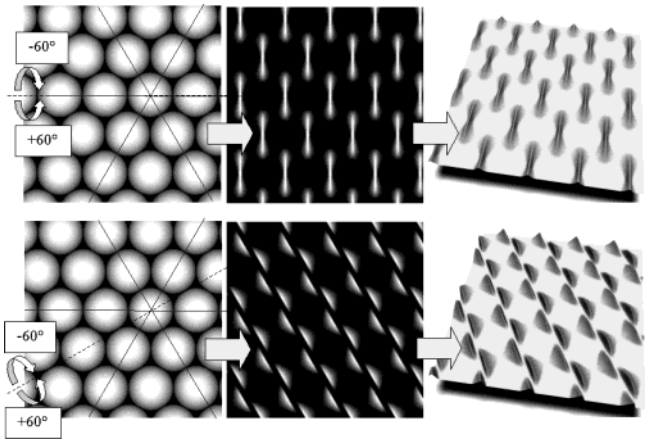

Figure 3. Simulation results for the evaporation through an hcp mask of ordered spheres, with the tilting angle oscillating between −60° to 60° during the process. The tilting axis is parallel the [100] direction (top), and [110] (bottom).

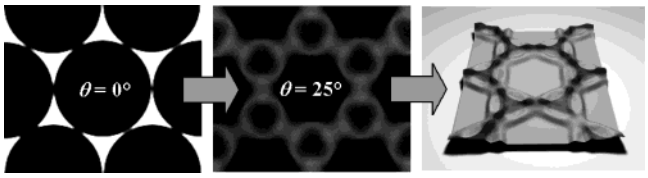

Figure 4. Two-step process: the first step is a perpendicular evaporation of one metal, and the second is the evaporation of second metal with sample rotation at $\theta = 25°$. The result is a complex bimetallic morphology.

the following formula for the shape (y vs x) of the shadow produced by a single PS sphere:

$$y = \frac{R \sin\theta \pm \sqrt{R^2 - x^2}}{\cos\theta} \tag{1}$$

where R is the sphere radius and θ the evaporation angle as defined in Figure 1.

The single sphere shadow is defined as a shadow function $S(x,y)$ equal to 0 for the area inside and 1 outside the curve

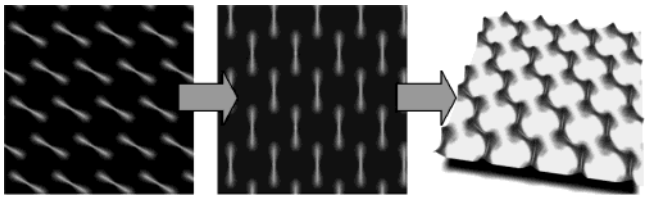

Figure 5. Two-step evaporation with tilting of the sample. The tilting axis is oriented with one of the symmetry axes during the first step, and with the other during the second step. This results in nanowires.

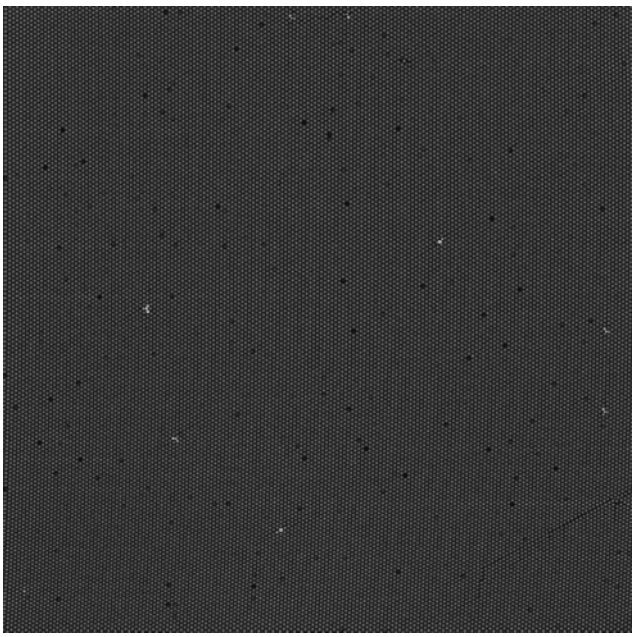

Figure 6. An hcp array of PS latex spheres 100 × 100 μm^2 assembled on a Si substrate.

described by eq 1. For many spheres, the combined shadow function $M(x,y)$ is calculated as follows:

$$M(x,y) = \Pi\, S(x - x_i, y - y_i) \tag{2}$$

where (x_i,y_i) represent the centers of the spheres in the array. In the dynamic case, we use the time dependent values of coordinates $x(t)$, $y(t)$, which are obtained from the values at time $t = 0$ by the following transformations:

$$\begin{bmatrix} x(t) \\ y(t) \end{bmatrix} = \begin{bmatrix} \cos(\omega t) & \sin(\omega t) \\ -\sin(\omega t) & \cos(\omega t) \end{bmatrix} \times \begin{bmatrix} x(0) \\ y(0) \end{bmatrix} \tag{3}$$

where ω is usually taken to be constant in the whole cycle, but in general it depends on the EBE parameters. The final, general expression for the deposited material density is

$$\mathrm{d}(x,y) = \sum \frac{I_0\, M(x(t),y(t);\theta(t))}{r(t)^2} \tag{4}$$

where $r(t)$ is the distance between the source and the sample. The sum is over all time steps in the whole cycle. The term $\mathrm{d}(x,y)$ can be easily compared with experimental AFM images.

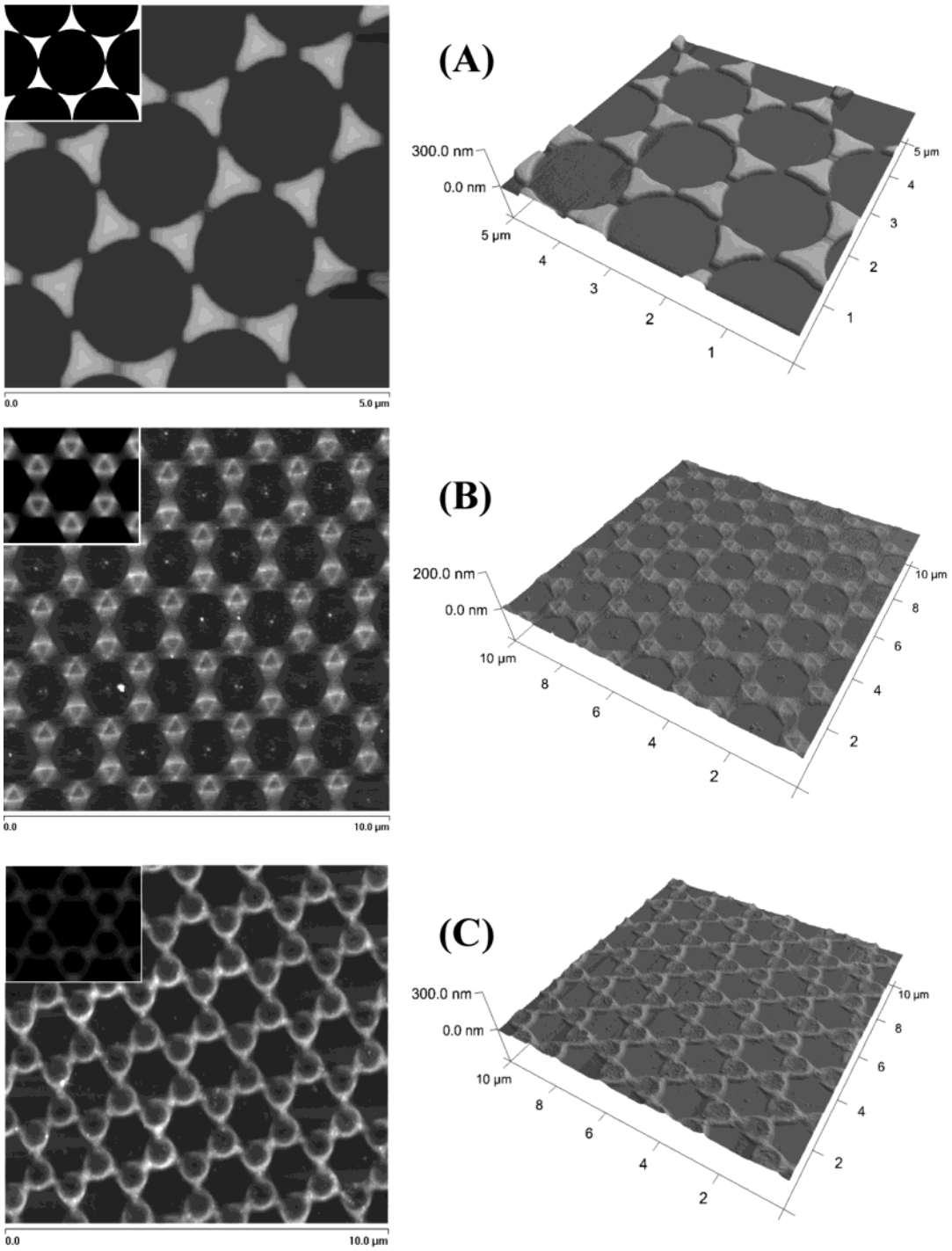

Figure 7. Comparison of simulation and experiment of evaporation with different θ values. Evaporation was masked with a 1710 nm PS latex monolayer on a Si substrate. The simulated particle shapes are shown in the insets on the corresponding AFM pictures. (A) 40 nm of Ni, $\theta = 0°$, (B) 40 nm of Ni, $\theta = 15°$, and (C) 150 nm of Cr, $\theta = 25°$. R = 1710 nm.

The main results of the simulations are presented in Figures 2−5. Figure 2 is a series of images calculated for different θ angles, varying from 0° (standard perpendicular evaporation) to 30°. The thickness of evaporated structures is represented by shades of gray (with black denoting zero deposition). A variety of structures can be obtained, such as reversed triangles for $\theta = 15°$, and an array of rods for $\theta = 30°$.

In another simulation we analyze the process that uses tilting of the sample during evaporation (by $\pm$ 60°) instead of rotation. The morphology of those structures depends on the initial orientation of the monolayer. Figure 3 (top) shows the case when the tilting axis is parallel to the [100] direction and Figure 3 (bottom) is for the tilting axis parallel to the [110] direction.

More complex morphologies can be obtained by a combination of these steps. For example, one can first evaporate the metallic triangles at $\theta = 0$, and then, in the second step, evaporate the same or another metal with rotation of the sample at $\theta = 25°$. This results in a double metallic structure shown in Figure 4.

In another example, we use the two-step evaporation with tilting of the sample. The tilting axis is oriented with one of the symmetry axes during the first step and with the other during the second step. This results in nanowires shown in Figure 5.

Experiment. Silicon substrates were obtained from CEMAT Silicon, Poland and cut into 1×1 cm^2 pieces. PS plane particles, Ø1710 nm (CV = 1.2%) were purchased from Microparticles, Germany, as a 10% aqueous dispersion, and PS plane particles Ø540 nm (CV = 2.2%) were purchased from IDC as 8% aqueous dispersion. Metal deposition has been done by evaporation using an e-beam evaporator, BAK 640, Unaxis, Switzerland.

Silicon substrates were cleaned in a solution of 7% NH_4OH/30% H_2O_2/Mili-Q water (1:1:5) by volume for 60 min at 80 °C then rinsed in Mili-Q water and dried in an argon stream. PS spheres (1710 nm) were used as received (10% aqueous dispersion), while 540 nm PS solutions were centrifuged to increase the concentration to about 30% in water. Furthermore, all particle suspensions were diluted by mixing with equal volumes of ethanol. Prepared ethanolic/water PS solutions were slowly applied on the surface of the water using a glass pipet. All PS monolayers were assembled inside a Ø15 cm Petri dish. The amount of solution that should be distributed to cover the whole water surface with a hcp monolayer is limited by the size of the Petri dish and the diameter of the used spheres. We have applied about 70% of this amount of solution to the surface of the water, leaving some place for stress relaxation and to avoid formation of cracks in the lattice during the next steps of the preparation. At this stage the monolayer had the biggest crystals of about 2 cm^2, with very irregular shapes. To promote the growth of large crystals, we have used gentle waves of the liquid medium by slow and careful vessel tilting. After this treatment, crystals of about 25 cm^2 were created showing clear diffraction colors. Finally, the monolayer was deposited on a substrate by slow water evaporation. After the drying process, various metals were deposited in an electron beam evaporator. All layers were evaporated in vacuum.

Experimental Results and Comparison with the Simulations. Using the procedure described in the previous section we produced 1×1 cm^2 samples with 100×100 μm^2 large, ordered areas without any structural defects (Figure 6).

We first demonstrate in Figure 7 the fabrication of the shapes simulated in Figure 2. The agreement between the simulation and the experimental result is excellent, confirming the validity of our assumptions.

Figure 8 demonstrates a structure obtained by using the procedure simulated in Figure 4. Again, an excellent corresponding result is obtained.

An interesting modification of this procedure is the process resulting in the structure shown in Figure 9. Here we use a two-step evaporation using spheres with $R = 540$ nm. First, we evaporate 150 nm Cr (with sample rotation) at $\theta \approx 25°$, followed by a normal evaporation ($\theta \approx 0°$) of 15 nm Ni.

In conclusion, we have presented computer simulations and experimental preparations showing the evolution of

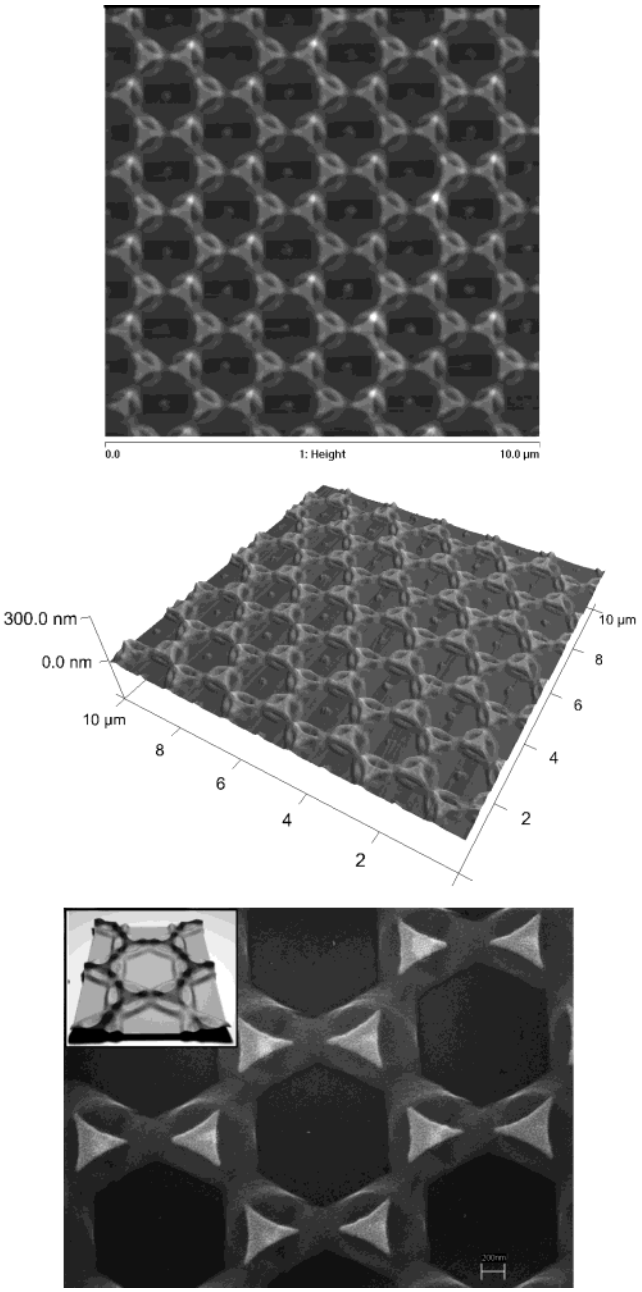

Figure 8. Comparison of simulation and experiment for the process of Figure 4. SEM image showing the result of a two-step evaporation process through a 1710 nm PS-latex mask: normal evaporation of 30 nm Au as the first step, and evaporation (with the sample rotation) at $\theta \approx 25°$ of 200 nm Cr as the second step. The inset shows the computer simulation.

triangular shapes into various complex structures that can be prepared by the shadow NSL. Large templates of a new kind of 2D ordered, submicron-sized particle have been demonstrated. Cup-like particles can find their utilization in immobilizing other particles in higher temperatures. They can also be used as a protection from oxidation. A large angle of evaporation allows us to decrease the size of intersphere spaces without depositing any material on the substrate. Therefore, metal particles evaporated in the following step will have a smaller size, while the distance between them remains constant. Such templates can be used as catalyst substrates for the production of ordered small diameter

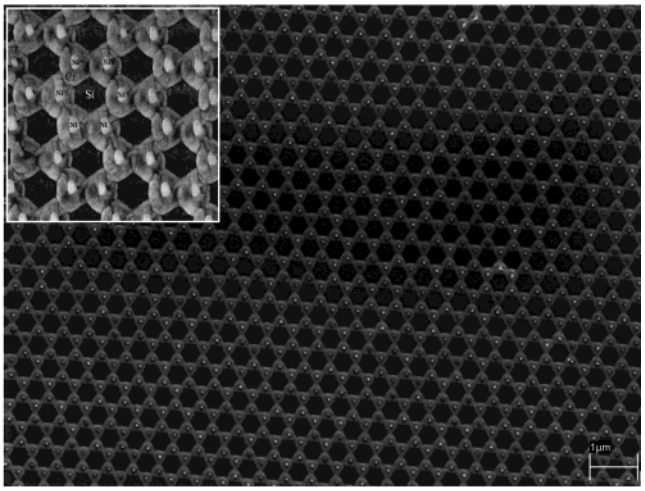

Figure 9. SEM image of a bimetallic structure, obtained by a two-step evaporation process. First step, evaporation of 150 nm Cr (with sample rotation) at $\theta \approx 25°$, followed by a normal evaporation ($\theta \approx 0°$) of 15 nm Ni. The inset shows the AFM tapping phase mode scan of the same sample, which shows well-separated Ni spots inside the cup-like Cr structures. The diameter of the mask spheres was 540 nm.

carbon nanotubes[11] or ZnO crystal[12] arrays. Furthermore, we have shown a novel way of making metallic nanorods and nanowires that are fixed on the substrate.

Currently, the minimum size of the deposited single nanoparticles that can be reached is 30 nm. The creation of the same (cm^2) nanostructures by e-beam lithography is time consuming and very expensive.

Acknowledgment. We thank Mr. Manfred Lacher for his assistance and for the use of clean-room facilities and Dr. Michael Hilgendorff for his advice and guidance with regard to this research. Additionally, we acknowledge the financial support of W.K. and A.K. within the EU-project, grant number: HPRN-CT-19999-00150.

References

(1) Deckman, H. W.; Dunsmir, J. H. *Appl. Phys. Lett.* **1982**, *41*, 377−379.
(2) Giersig, M.; Mulvaney, P. *Langmuir* **1993**, *9*, 3408.
(3) Deckman, H. W.; Dunsmuir, J. H. *Appl. Phys. Lett.* **1982**, *4*, 377.
(4) Hulteen, J. C.; Van Duyne, R. P. *J. Vac. Sci. Technol. A* **1995**, *3*, 1553.
(5) Winzer, M.; Kleiber, M.; Dix, N.; Wiesendanger, R. *Appl. Phys. A* **1996**, *63*, 617.
(6) Micheletto, R.; Fukuda, H.; Ohtsu, M. *Langmuir* **1995**, *11*, 3333.
(7) Burmeister, F.; Badowsky, W.; Braun, T.; Wieprich, S.; Boneberg, J.; Leiderer, P. *Appl. Surf. Sci.* **1999**, *144−145*, 461.
(8) Denkov, N. D.; Velev, O. D.; Kralchevsky, P. A.; Ivanov, I. B.; Yoshimura, H.; Nagayama, K. *Langmuir* **1992**, *8*, 3183.
(9) Rybczynski, J.; Ebels, U.; Giersig, *M. Colloids Surf. A: Physicochem. Eng. Aspects* **2003**, *219*, 1.
(10) Haynes, C. L.; Van Duyne, R. P. *Nano Lett.* **2003**, *7*, 939.
(11) Kempa, K.; Kimball, B.; Rybczynski, J.; Huang, Z. P.; Wu, P. F.; Steeves, D.; Sennett, M.; Giersig, M.; Rao, D. V. G. L. N.; Carnahan, D. L.; Wang, D. Z.; Lao, J. Y.; Li, W. Z.; Ren, Z. F. *Nano Lett.* **2003**, *3*, 13.
(12) Wang, X.; Summers, C. J.; Wang, Z. L. *Nano Lett.* **2003**, *4*, 423.

NL049361T